Using NWP Reanalysis Data for Radiometric Calibration in Electromagnetic Wave Propagation Experiments

Lorenzo Luini and Carlo Capsoni

Abstract—**Extensive datasets distributed by the European Centre for Medium-range Weather Forecast (ECMWF) are used to calculate retrieval coefficients for dual-channel radiometers in 14 sites spread across Europe, where databases of high-resolution RAdiosonde OBServations (RAOBS) are available. RAOBS are employed as the reference to assess the results obtained from ECMWF products, both in terms of single radiometric coefficients and in terms of statistics of integrated water vapor, integrated liquid water and total atmospheric attenuation retrieved from radiometric measurements collected in one site close to Milan, Italy. The findings suggest that NWP products can be successfully used to calibrate radiometers when no appropriate RAOBS data are available.**

Index Terms—**Numerical Weather Predictions, radiometry, atmospheric radio wave propagation.**

I. Introduction

The design of modern satellite communication systems is becoming more and more critical as the operational frequency is gradually shifting to the Ka band and beyond. In fact, at these bands the detrimental impact of the atmosphere on radio waves increases considerably such that, besides rain, which always plays the dominant role in the microwave and millimeter wave bands (though its occurrence is limited to approximately 1-10% of the time in a year), also clouds and gases have to be taken into account and their impact on the system accurately estimated [1].

In order to support the huge efforts devoted to the development of theoretical models for the prediction of clouds, gases and hydrometeors impact on Earth-space links, the most effective means is to use as reference ground receivers measuring stable unmodulated signals (beacons) transmitted by payloads onboard satellites on geostationary orbits (but also on medium/low orbits in the near future) [2] . These activities, examples of which are the SIRIO, OLYMPUS, ITALSAT and Alphasat projects in Europe, and the ATS, COMSTAR and ACTS programs in USA, consist in recording the beacon signal, likely to be supported by ancillary measurements sounding the state of the atmosphere [3]. Additional instruments are in fact required to provide an independent estimation of the actual atmospheric attenuation, and to "calibrate" the signal received from beacons [4].

Among ancillary instruments, radiometers are extremely useful to this aim, as they provide the integrated water vapor (V) and liquid water (L) contents as well as the total atmospheric attenuation along the path in non-rainy conditions at any frequency once the proper retrieval coefficients are known. In turn, these quantities can be derived from RAdiosonde OBServations (RAOBS) that sound the vertical structure of the atmosphere [5]. Unfortunately radiosondes are routinely launched only at specific sites (mostly airports) and, thus, may not be available close enough (e.g. roughly less than 50 km) to the site where the radiometer is installed.

This contribution investigates whether and to what extent Numerical Weather Predictions (NWPs) can be successfully used to calculate the coefficients needed to estimate V and L, as well as the total atmospheric attenuation in rain-free conditions, from radiometric brightness temperatures measured at two (or more) frequencies. The NWP data used in this work are made available by the European Centre for Medium-range Weather Forecast (ECMWF) [6]. Whilst worldwide coverage and increasing accuracy definitely represent appealing features of NWP data (especially reanalysis ones), on the other side, their coarse horizontal spatial resolution might limit their effectiveness in radiometric applications. In order to take into account this issue, and to assess to what extent NWP data are suited for the mentioned task, results obtained from ECMWF products are compared to those achieved from a reference set of RAOBS data collected across Europe. Specifically, Section II presents the atmospheric products (RAOBS and NWP) used in this work, together with brightness temperature data collected by the dual-channel radiometer installed at the experimental station of Spino d'Adda, Italy. Section III proposes a methodology aimed at maximizing the accuracy of radiometric calibration coefficients as derived from NWP data, which basically consists in properly truncating or extending such profiles based on the altitude of the reference site where the radiometer is installed. Section IV first illustrates the procedure to calculate the radiometric coefficients, and afterwards compares and evaluates the results obtained from

Manuscript received XXXX.

Lorenzo Luini and Carlo Capsoni are with the Dipartimento di Elettronica, Informazione e Bioingegneria, Politecnico di Milano, Piazza Leonardo da Vinci, 35, 20133, Milano, Italy, and with the Istituto di Elettronica e di Ingegneria dell'Informazione e delle Telecomunicazioni (IEIIT), CNR, Milano, Italy (e-mail: lorenzo.luini@polimi.it).

RAOBS and NWP data, both in terms of single coefficients as well as in terms of statistics of integrated water vapor, integrated liquid water and total atmospheric attenuation retrieved from the radiometric data mentioned above. Finally, Section V draws some conclusions.

II. Datasets

A. Radio soundings

RAOBS data used here are part of the FERAS (FUB-ESA Radiosonde, being FUB the acronym for Fondazione Ugo Bordoni) dataset which has been assembled by the European Space Agency (ESA) using an extensive NCAR (National Center for Atmospheric Research) database [7]. The dataset consists of high-resolution (10/20 m for the lowest layers) vertical profiles of pressure (*P*), relative humidity (*RH*) and temperature (*T*), collected routinely twice a day (0 and 12 UTC) for ten years (1980-1989) in non-rainy conditions. Data are available for 14 sites spread across Europe, from Sodankyla, Finland, to Trapani, Italy. It is worth noting that the sites are characterized by very different climates, ranging from cold continental to hot Mediterranean. All the data contained in the FERAS database have been accurately validated using original NCAR quality control marks, if present, and basic plausibility and inconsistency checks [7].

B. Meteorological reanalysis

The ECMWF provides atmospheric datasets produced as output of global-scale NWP models. Both forecasts and reanalyses are available, the latter being a reassessment of NWP outputs based on concurrent measurements. Specifically, the ERA 40 and the ERA Interim reanalysis data used here (1980-1989 period concurrent with the one of RAOBS data) include 60 vertical atmospheric layers (extending up to 55/60 km) sampled every six hours on a latitude/longitude grid with 1.125°×1.125° and 0.75°×0.75° spatial detail, respectively [6]. The vertical resolution of raw data ranges from a few tens of meters close to the ground to about 700 m around 10-km height.

C. Radiometric measurements

Brightness temperatures have been collected with 1-second sample time for seven years by a dual-channel radiometer (manufactured by Elecktronic Centralen, 23.8 GHz and 31.6 GHz, 37.7° elevation angle) installed at the experimental station of Spino d'Adda (45.4° N, 9.5° E, altitude 84 m a.m.s.l.), 20 km east of Milano/Linate. This dataset is used here as a further means to assess the suitability of ECMWF reanalysis data for radiometric calibration.

III. Atmospheric Vertical Profiles

As explained in detail in section IV.A, the calibration of radiometers requires knowledge on the local state of the atmosphere, which, in turn, can be adequately characterized by using vertical profiles of pressure, temperature and relative humidity. When proper RAOBS data are not available, ECWMF profiles represent a promising alternative, which, however, is associated to some potential limitations.

While the vertical sampling of ECMWF profiles has reached a fairly good resolution (20 m to 30 m for the lowest layers), the horizontal detail is relatively coarse. In fact, all ECMWF reanalysis values are averaged over a regular latitude/longitude grid, which not only means that horizontal gradients of *P-RH-T* are filtered out, but also that the lowest layer height h_0 in the profiles depends on the orography surrounding the reference site. Therefore, h_0 is expected to change from dataset to dataset and from site to site because of the different position of the pixel of interest, as well as of its size: throughout the paper the NWP profile considered is the one associated to the pixel containing the site. These aspects are clarified in Fig. 1, where Milano/Linate airport (black square marker) and the four surrounding ECMWF pixels are overlaid onto the orographic map of north-western Italy (digital elevation maps elaborated by the U.S. Geological Survey [8]). In both cases Milano/Linate falls in the south-western pixel but, due to the different resolution of the two NWP databases, the lowest layer is associated to $h_0 \approx 490$ m a.m.s.l. and to $h_0 \approx 180$ m a.m.s.l. for the ERA 40 and the ERA Interim, respectively.

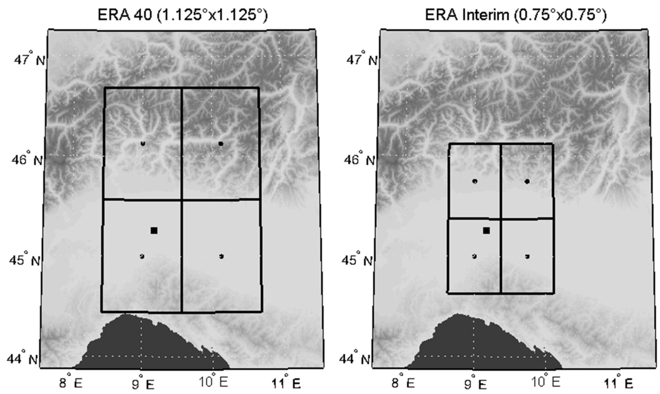

Fig. 1. Position of Milano/Linate (black square marker) and of the surrounding ECMWF pixels (ERA 40 on the left side and ERA Interim on the right side). Digital elevation maps provided by U.S. Geological Survey (flat areas in white, peaks in darker shades of gray).

While the impact of coarse spatial detail of NWP data for radiometric calibration cannot be estimated a priori (neither can it be easily mitigated), the difference between h_0 and the reference site altitude h_s (e.g. 105 a.m.s.l. for Milano/Linate airport), $\Delta h = h_0 - h_s$, needs to be taken into due account: indeed, disregarding low vertical layers might have a relevant impact in the calculation of calibration coefficients and on any derived quantity. On the contrary, if h_0 is lower than the reference site altitude h_s the NWP profiles can be simply interpolated and truncated.

If $h_0 > h_s$, the information close to the ground needs to be recovered in different ways depending on the atmospheric quantity considered. This task is relatively easy for pressure, whose vertical profile tends to be quite regular and is typically modeled as (*h* is the height in km above a.m.s.l.):

This is the author's version of an article that has been published in this journal. Changes were made to this version by the publisher prior to publication.
The final version of record is available at http://dx.doi.org/10.1109/TAP.2015.2511790

$$P(h) = P_G\, e^{-h/h_P} \tag{1}$$

where P_G is the pressure at sea level (hPa) and h_P regulates the slope of (1). The NWP-derived pressure profiles are extended by adding a fictitious ground layer whose height corresponds to the reference site altitude h_s and whose pressure P_s is obtained by first fitting (1) to the NWP profile for the derivation of P_G and h_P, and then by setting $P_s = P(h = h_s)$, as shown, for example, in Fig. 2.

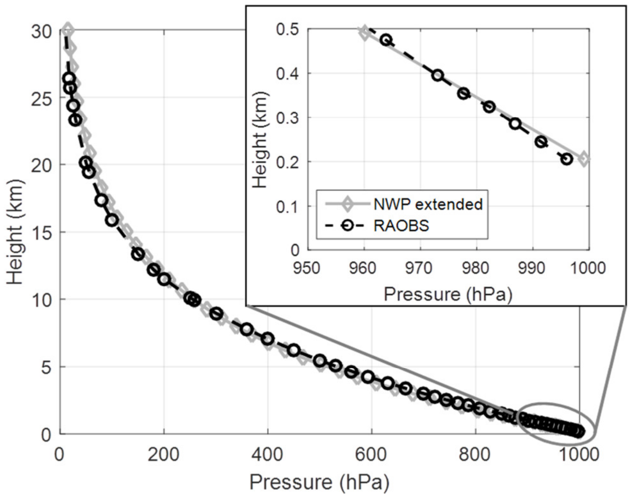

Fig. 2. Example of the extension of an ERA 40-derived pressure profile (pixel centered in 45° N and 9° E) using the exponential expression in (1) (gray line with diamonds, P_G = 1028 hPa and h_P = 7.2 km) and comparison with the concurrent RAOBS profile collected at Milano/Linate airport. The inset offers a zoom on the profiles to better appreciate the predicted and reference P value associated to 205 m a.m.s.l., i.e. the first layer available from the RAOBS dataset (100 m above h_s = 105 m a.m.s.l.).

Temperature varies more than pressure with height, and can be subject to strong inversions, also close to the ground. Nevertheless, on average, we assume the lapse rate ΔT to be constant: in fact, in the International Standard Atmosphere (ISA), ΔT is 6.49 °C/km from the sea level up to approximately 11 km [9], while ΔT = 0 °C/km between 11 km and 20 km. As ΔT might vary considerably when the conditions of standard stationary atmosphere are not met (e.g. typical ΔT = 9.8 °C/km and 5 °C/km for unsaturated and saturated air, respectively [10]), for each profile, ΔT is inferred by linearly interpolating the temperature profile up to h_M = 8 km, which, in turn, as shown for example in Fig. 3, allows the simple estimation of T_s (temperature value at the reference altitude h_s), as:

$$T_s = T(h = h_s) = T_0 + \Delta T \Delta h = T_0 + \Delta T\left(h_0 - h_s\right) \tag{2}$$

In (2), T_0 is the temperature associated to the lowest NWP level at height h_0. The limit height h_M = 8 km was chosen, on one side, based on the ISA (constant lapse rate up to 11 km) and, on the other side, as a result of the visual inspection of several profiles of T used in this work, which sometimes deviate from the constant lapse rate model for heights above 8 km.

The third parameter, relative humidity, varies significantly with height, and follows quite irregular trends. On the contrary, the vertical profile of water vapor density v, which is linked to RH, is typically modeled using an exponential profile:

$$v(h) = v_G\, e^{-h/h_v} \tag{3}$$

In (3), v_G is the water vapor content at sea level (g/m^3) and h_v is the exponential decay rate, typically much steeper than h_P in (1) (v tends to zero for h around 10/12 km). Thus, similarly to pressure, each NWP-derived v profile can be first fitted to determine v_G and h_v (using the full profile), and afterwards extended to the reference site by setting $v_s = v(h = h_s)$. The final step to complete the profiles extension is to calculate the relative humidity at h_s as:

$$RH_s = 100\, E/E^* \tag{4}$$

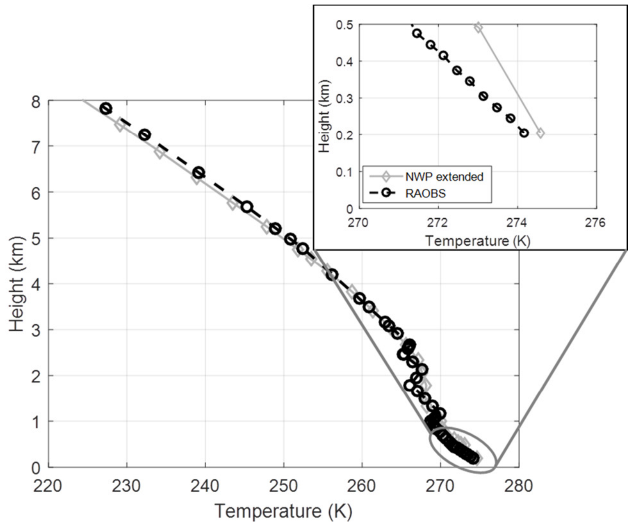

Fig. 3. Example of the extension of an ERA 40-derived temperature profile (pixel centered in 45° N and 9° E) using the linear expression in (2) (gray line with diamonds, ΔT = 5.45 °C/km) and comparison with the concurrent RAOBS profile collected at Milano/Linate airport. The inset offers a zoom on the profiles to better appreciate the predicted and reference T value associated to 205 m a.m.s.l., i.e. the first layer available from the RAOBS dataset (100 m above h_s = 105 m a.m.s.l.).

E and E^* in (4) are the partial pressure of water vapor and the equilibrium vapor pressure of water. The former is related to relative humidity as [10]:

$$E = \frac{v_s T_s}{216.72} \tag{5}$$

being T_s expressed in K and v_s in g/m^3, while the latter can be calculated using several formulations available in the literature, the most common one being the Goff-Gratch equation [11] (it is recommended for use by the World Meteorological Organization). Fig. 4 shows a sample ERA 40-derived profile of relative humidity, extended using the methodology outlined above and compared with the concurrent profiles measured by the Milano/Linate radiosonde.

This is the author's version of an article that has been published in this journal. Changes were made to this version by the publisher prior to publication.
The final version of record is available at http://dx.doi.org/10.1109/TAP.2015.2511790

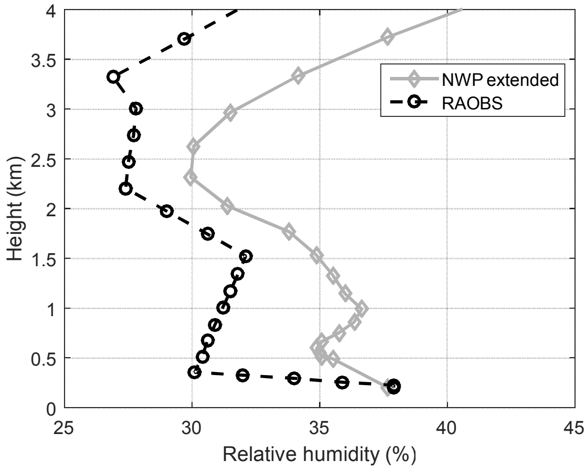

Fig. 4. Example of the extension of an ERA 40-derived relative humidity profile (pixel centered in 45° N and 9° E, gray line with diamond marker) and comparison with the concurrent RAOBS profile collected at Milano/Linate airport.

The accuracy of the proposed approach for NWP vertical profile extension can be evaluated by using as reference the full dataset of concurrent RAOBS. To this aim, the average (Eε_Y) and root mean square (RMSε_Y) of the following error figure ε_Y are used:

$$\varepsilon_Y = Y_{s,NWP} - Y_{s,RAOBS} \tag{6}$$

where $Y_{s,NWP}$ and $Y_{s,RAOBS}$ are the values as obtained from the extended NWP profile and as measured by the radiosonde, while Y is P, RH or T. Equation (6) is calculated only on the values associated to the lowest RAOBS level, i.e. the ones obtained for each NWP profile using the extension procedure described above.

Examples of Eε_Y and RMSε_Y are shown, as function of the site where RAOBS data are available, in Fig. 5 and Fig. 6 for temperature and relative humidity, respectively, using the ERA 40 dataset and the full measurements period (1980-1989). In addition, Table I summarizes the overall error in predicting ground values of P, T, RH and v using both NWP datasets.

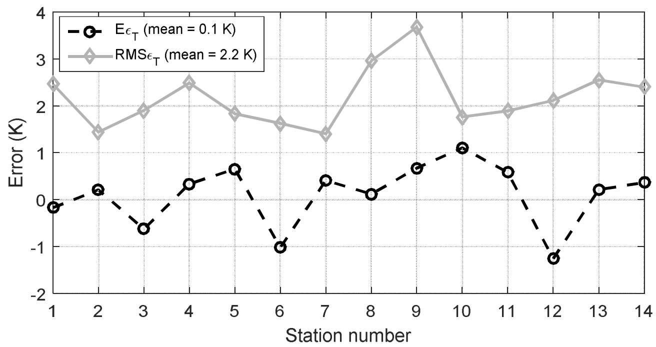

Fig. 5. Eε_T and RMSε_T for all the FERAS stations where RAOBS have been collected; the average value of Eε_T and RMSε_T over tha whole database is reported in the figure legend.

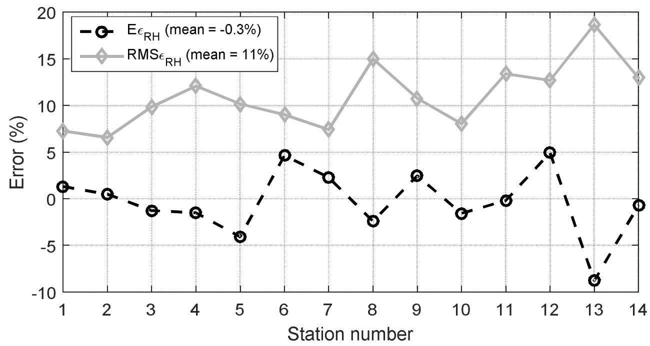

Fig. 6. Eε_{RH} and RMSε_{RH} for all the FERAS stations where RAOBS have been collected; the average value of Eε_{RH} and RMSε_{RH} over tha whole database is reported in the figure legend.

Results, sorted as a function of increasing Δh in Fig. 5 and Fig. 6 (up to 458 m for ERA 40, and to 316 m for ERA Interim), indicate good prediction accuracy, with very satisfactory values of RMSε_Y, slightly higher for relative humidity, as expected due to its larger space and time variability. Also, results turn out to be almost independent of Δh: this finding corroborates the use of the proposed profile extension approach, which appears to be effective also for larger differences between the NWP pixel height h_0 and site altitude h_s. This is also confirmed by the overall bias Eε_Y reported in Table I, which is close to zero for all the atmospheric variables.

TABLE I. OVERALL ERROR IN PREDICTING P, T, RH AND V ASSOCIATED TO THE SITE REFERENCE ALTITUDE

		ERA 40	ERA Interim
***P* (hPa)**	**Eε_P**	0.5	-0.2
	RMSε_P	11.9	12.2
***T* (K)**	**Eε_T**	0.1	-0.1
	RMSε_T	2.2	2.1
***RH* (%)**	**Eε_{RH}**	-0.3	0.1
	RMSε_{RH}	11	11.5
***v* (g/m^3)**	**Eε_v**	0	0
	RMSε_v	1.2	1.2

IV. RADIOMETRIC CALIBRATION COEFFICIENTS

A. *Calculation procedure*

The first step towards the derivation of the radiometric calibration coefficients using vertical profiles of *P-RH-T* involves the use of a cloud detection algorithm to quantify the cloud water content. Specifically, we make use of the TKK (Teknillinen korkeakoulu - Helsinki University of Technology) model to identify and characterize clouds in terms of liquid and ice water contents (LWC and IWC, respectively) in g/m^3 [12].

Afterwards, the well-established mass absorption model proposed by Liebe (MPM93 [13]) is employed to derive all the propagation quantities necessary to calibrate radiometric retrievals (at the radiometric frequencies 23.8 and 31.6 GHz), i.e.:

- $A_L(f)$ and $A_V(f)$, the attenuation due to cloud liquid water and water vapor along the profile (dB), respectively;
- $A_{ox}(f)$, the attenuation due to oxygen along the profile (dB);
- $T_{mr}(f)$, the mean radiating temperature of the medium (K).

By cumulating the results obtained from all the vertical profiles available for a given dataset, the mass absorption coefficients for water vapour and liquid water (k_V and k_L, respectively) are calculated as the slope of the linear curve fitting the A_V/V and A_L/L relationships, i.e.:

$$A_V = k_V\,V \quad \text{and} \quad A_L = k_L\,L \tag{7}$$

Fig. 7 shows k_L = 0.8902 dB/mm as calculated, for example, for 31.6 GHz and from the RAOBS data collected at Milano/Linate using the TKK and MPM93 models (4966 *P-RH-T* vertical profiles), while Fig. 8 summarizes the whole process for the derivation of the radiometric calibration coefficients.

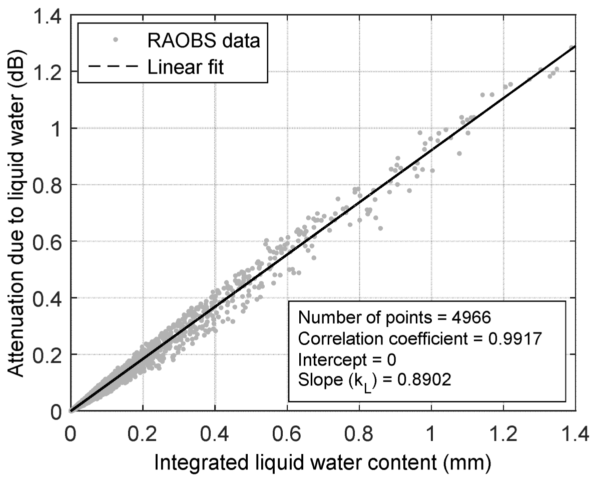

Fig. 7. Mass absorption coefficient for liquid water, k_L, calculated using RAOBS data collected at Milano/Linate airport (TKK and Liebe MPM93 models) at f = 31.6 GHz.

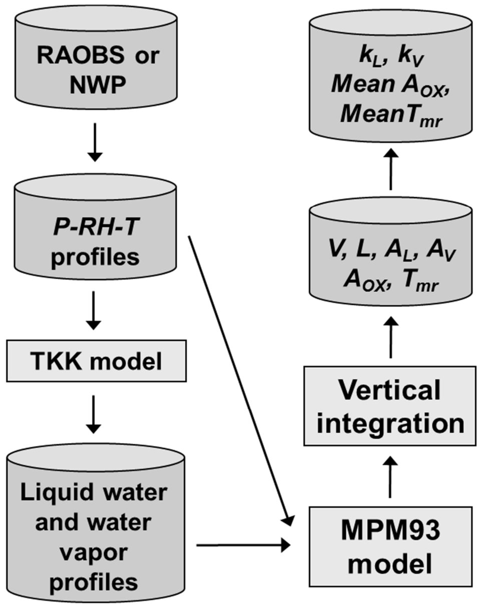

Fig. 8. Full process for the derivation of the radiometric calibration coefficients from RAOBS or NWP vertical profiles of pressure, temperature and relative humidity.

B. Results

The suitability of NWP vertical profiles for the calculation of radiometric coefficients is illustrated in Fig. 9, Fig. 10, Fig. 11 and Fig. 12 (lines labelled “no correction” refer to the profiles as originally provided by ECMWF, while the other two lines refer to the application of the profile extension procedure), which show, for each FERAS station, examples of the relative error between NWP- and RAOBS-derived radiometric coefficients (90° elevation angle): specifically, k_V at 23.8 GHz, k_L at 31.6 GHz, the mean value of A_{ox} ($\overline{A}_{ox}$) at 23.8 GHz and the mean value of T_{mr} ($\overline{T}_{mr}$) at 31.6 GHz. The figure legend also reports the average (E) and root mean square (RMS) values of the error.

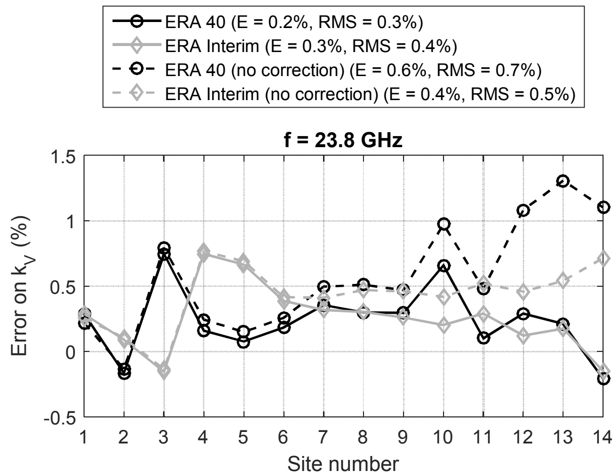

Fig. 9. Error in estimating k_V at 23.8 GHz using NWP profiles for all the FERAS stations. Results sorted as a function of increasing Δh.

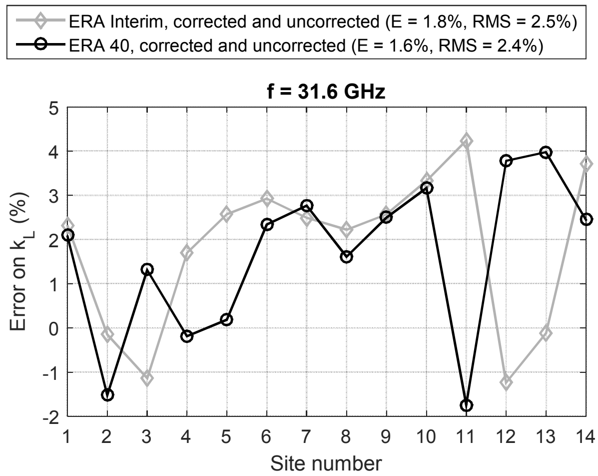

Fig. 10. Error in estimating k_L at 31.6 GHz using NWP profiles for all the FERAS stations. Results sorted as a function of increasing Δh.

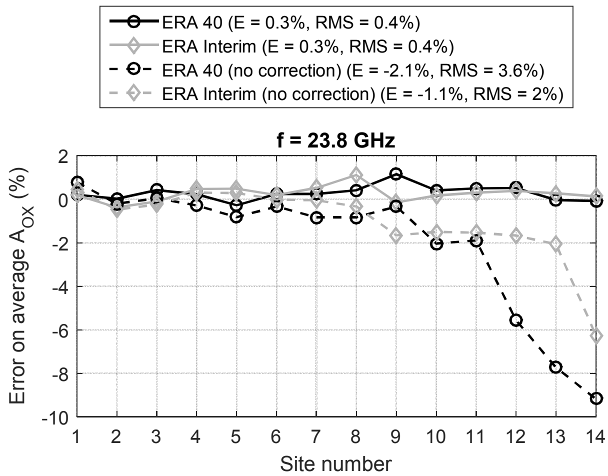

Fig. 11. Error in estimating $\overline{A}_{ox}$ at 23.8 GHz using NWP profiles for all the FERAS stations. Results sorted as a function of increasing Δh.

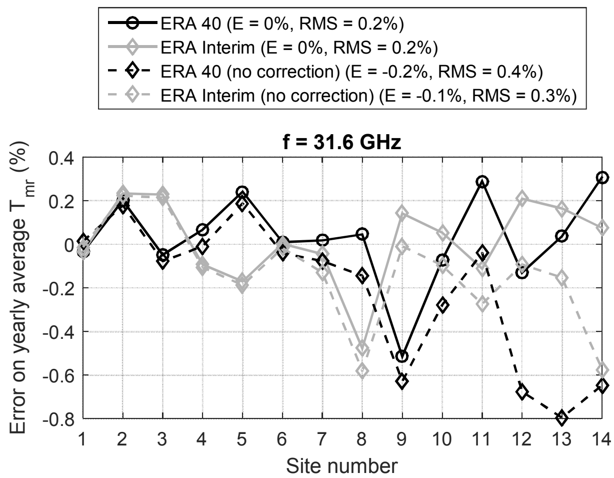

Fig. 12. Error in estimating $\overline{T}_{mr}$ at 31.6 GHz using NWP profiles for all the FERAS stations. Results sorted as a function of increasing Δh.

Results, once again sorted as a function of increasing Δh, allow appreciating the positive impact of the proposed NWP profile extension approach, whose effectiveness, as expected, is more and more marked as Δh grows: the first 9 sites, for which the effects of the correction is less significant, are associated to Δh values up to 70 m (for both NWP databases); the benefit of the profile extension is more visible for sites 10 and 11, for which 110 m $\leq \Delta h \leq$ 120 m (ERA 40) and 80 m $\leq \Delta h \leq$ 90 m (ERA Interim); finally the most relevant impact can be appreciated for sites 12 to 14, where Δh extends up to 490 m (ERA 40) and 320 m (ERA Interim). The performance scores in the figures show that no changes occur in k_L (clouds typically lie at altitudes higher than the h_0 values involved in this work), that there is a marginal improvement in the coefficients accuracy for k_V and $\overline{T}_{mr}$, and that the largest variation is associated to $\overline{A}_{ox}$. Moreover, while after the profile extension the difference in accuracy obtained from using ERA 40 or ERA Interim is practically negligible, the latter should be preferred to the former if no profile extension is applied.

C. Radiometric inversions

The conclusive test on the procedure of ECMWF profile extension is given by its impact on the derivation of the statistics of V, L and tropospheric attenuation in non-rainy conditions at different frequencies (we have chosen the ones of the current Alphasat propagation experiment, i.e. f =19.7, 39.6 and 48 GHz) [14].

As it is well known, radiometers allow to estimate the total path attenuation $A(f)$ (in dB) from the knowledge of $\overline{T}_{mr}(f)$ and the measured brightness temperature $T_B(f)$ [4]:

$$\begin{aligned} A(f_1) &= \overline{A}_{ox}(f_1) + k_V(f_1)\,V + k_L(f_1)\,L \\ A(f_2) &= \overline{A}_{ox}(f_2) + k_V(f_2)\,V + k_L(f_2)\,L \end{aligned} \tag{8}$$

In (8):

$$A(f_i) = 10\log_{10}\left(\frac{\overline{T}_{mr}(f_i) - T_C}{\overline{T}_{mr}(f_i) - T_B(f_i)}\right) \tag{9}$$

where T_C is the cosmic background temperature, typically set to 2.73 K in the microwave region, whilst f_1 = 23.8 GHz and f_2 = 31.6 GHz in this work.

The inversion of (8) leads to the estimation of V and L (expressed in mm) and, once V and L are known, equation (8) can be applied to estimate the atmospheric attenuation at any frequency, provided that k_L, k_V and $\overline{A}_{ox}$ are available at that frequency too. In this test we have excluded measurements under rainy conditions by applying the procedure based on the ratio of the brightness temperatures at 23.8 and 31.6 GHz proposed in [15], where it is shown that the parameter

$$R = \left[T_B(31.6\text{ GHz}) - k_R\right] / T_B(23.8\text{ GHz}) \tag{10}$$

is appropriate to identify non-rainy conditions by setting $R < 0.95$ and $k_R = 11.917$.

Fig. 13 shows the Complementary Cumulative Distribution Functions (CCDFs) of V (top side) and L (bottom side), derived by inverting the 1-minute averaged brightness temperatures collected by the radiometer installed at Spino d'Adda (seven-year period). The different curves correspond to the use in (8) of the sets of coefficients obtained from RAOBS data and from NWP data with no profile extension.

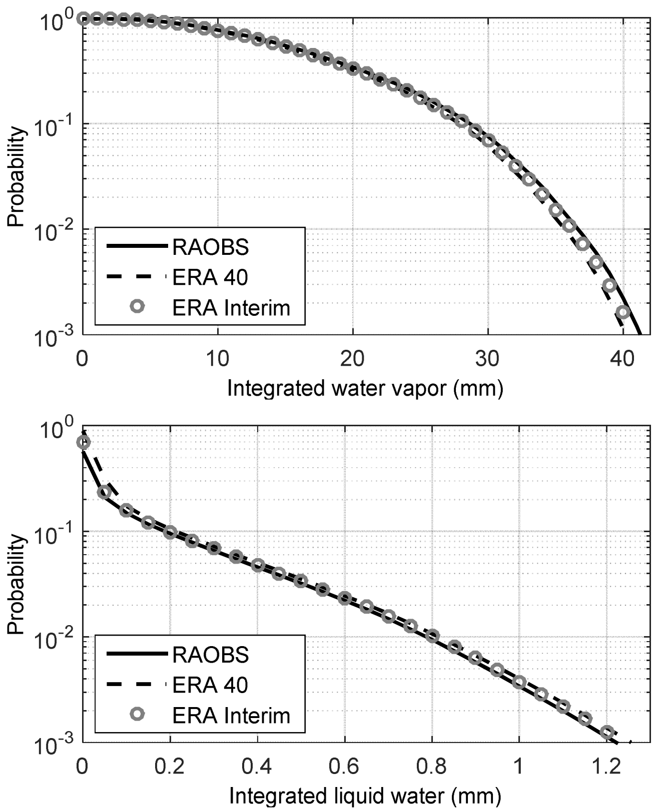

Fig. 13. CCDFs of V (top side) and L (bottom side) derived by inverting the 1-minute average brightness temperatures collected by the Spino d'Adda radiometer. The three different curves in each graph correspond to the use in (8) of the sets of coefficients obtained from RAOBS data and from NWP data with no profile extension.

The discrepancy among the curves in Fig. 13 is quantified according to the following error figures ($10^{-3} \leq P \leq 1$):

$$\begin{aligned} \varepsilon_V(P) &= 100\left[V_E(P) - V_R(P)\right]/V_R(P) \\ \varepsilon_L(P) &= 100\left[L_E(P) - L_R(P)\right]/L_R(P) \end{aligned} \tag{11}$$

where $V_E(P)$ and $L_E(P)$ are the V and L radiometric estimates at probability level P achieved using ECMWF profiles, whilst $V_R(P)$ and $L_R(P)$ are the equiprobable V and L values derived from RAOBS data.

The first two lines of Table II indicates that the use of either ECMWF dataset leads to a slight underestimation of V and slight overestimation of L. ERA Interim data allow a more accurate retrieval than ERA 40 data, which reflects the findings in Fig. 9, Fig. 10, Fig. 11 and Fig. 12 when no profile correction is applied.

TABLE II. AVERAGE (E) AND ROOT MEAN SQUARE (RMS) VALUES OF THE RETRIEVAL ERROR FOR V AND L

	E (%)		RMS (%)	
	V	***L***	***V***	***L***
ERA 40 (no correction)	-2.1	5.9	2.1	12.3
ERA Interim (no correction)	-1.1	0.7	1.1	4.2
ERA 40	-0.6	-2.5	0.6	2.9
ERA Interim	-1.0	-1.2	1.0	2.2

The agreement among the CCDFs of V and L increases even more when the coefficients derived from extended NWP profiles are employed. This is confirmed by the curves depicted in Fig. 14 and by the E and RMS values reported in the third and fourth lines of Table II, which clearly indicate that, after applying the NWP profiles extension, the ERA 40 and ERA Interim datasets basically provide the same accuracy in the retrieval of V and L.

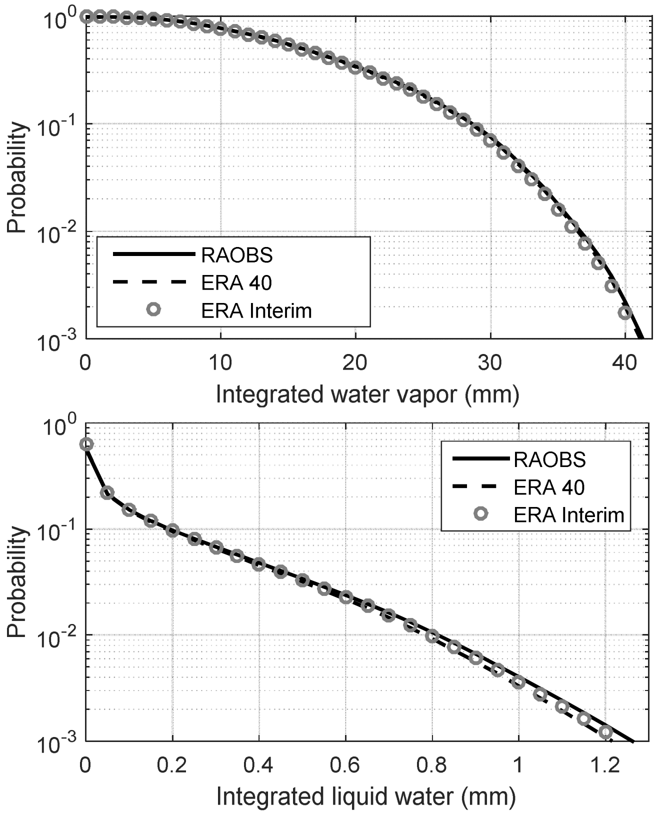

Fig. 14. CCDFs of V (top side) and L (bottom side) derived by inverting the 1-minute average brightness temperatures collected by the Spino d'Adda radiometer. The three different curves in each graph correspond to the use in (8) of the sets of coefficients obtained from RAOBS data and from extended NWP data.

Finally, Table III reports the accuracy in estimating the CCDF of total attenuation due to oxygen, water vapor and clouds for the Alphasat operational frequencies f = 19.7, 39.6

and 48 GHz: overall, errors are very small, and they decrease even more with the application of the NWP profile extension.

TABLE III. AVERAGE (E) AND ROOT MEAN SQUARE (RMS) VALUES OF THE RETRIEVAL ERROR FOR ATMOSPHERIC ATTENUATION

	E (%)			RMS (%)		
	$A_{19.7}$	$A_{39.4}$	A_{48}	$A_{19.7}$	$A_{39.4}$	A_{48}
ERA 40 (no correction)	-0.1	0.3	-2.8	0.5	0.4	3
ERA Interim (no correction)	-0.3	-0.1	-0.7	0.3	0.2	0.7
ERA 40	0	-0.1	-0.1	0.2	0.2	0.4
ERA Interim	-0.2	-0.2	-0.2	0.3	0.3	0.4

V. CONCLUSIONS

This work discusses the effectiveness and limitations of the ERA 40 and ERA Interim reanalysis data provided by the ECMWF for the calibration of radiometric retrieval products, which, in turn, are of importance to support scientific electromagnetic wave propagation experiments. Tests were performed using 10 years of ERA 40 and ERA Interim *P-RH-T* vertical profiles. The 14 sites of interest are spread across Europe where a long-term (10 years) dataset of RAOBS is available and has been used as reference to calculate radiometric coefficients for a dual-channel radiometer (23.8 and 31.6 GHz). In order to address the possible difference between the lowest layer in ECMWF profiles and the actual altitude of the reference site, Δh, a simple *P-RH-T* profile correction approach was proposed, which was found to be very effective, when tested against the concurrent RAOBS profiles, to derive accurate radiometric retrieval coefficients. Results turned out to be almost independent of the NWP dataset used if the profile correction is applied, while ERA Interim has shown to provide the best accuracy if no correction is used. The derived coefficients have been also employed to retrieve V, L and the total atmospheric attenuation A from the extensive dataset of brightness temperatures collected by the Spino d'Adda radiometer (20 kilometers east of Milano/Linate). Results indicate a very small discrepancy (almost zero with the application of the height correction) among the CCDFs of V, L and A obtained using the coefficients from the three sources. Overall, the findings obtained in this work definitely suggest that NWP datasets can be successfully used to calibrate radiometers when no proper RAOBS are available close enough (roughly 50 km) from the site where the instrument is installed. This, in turn, is of key importance to support electromagnetic wave propagation experiments such as the ongoing Alphasat project.

ACKNOWLEDGMENT

The authors would like to thank the ECMWF for producing and making freely available meteorological reanalysis data, Dr. Antonio Martellucci from ESA for granting access to the FERAS database and the U.S. Geological Survey for distributing global digital elevation maps.

REFERENCES

[1] C. Riva, C. Capsoni, L. Luini, M. Luccini, R. Nebuloni, A. Martellucci, "The Challenge of Using the W Band in Satellite Communication," *Int. J. Satell. Commun. Network.* 2014; 32:187–200.

[2] A. Paraboni, C. Riva, L. Valbonesi, M. Mauri, "Eight Years of ITALSAT Copolar Attenuation Statistics at Spino d'Adda," *Space Communications*, Vol. 18, No. 1-2, 2002, pp. 59-64.

[3] C. Capsoni, L. Luini, A. Paraboni, C. Riva, A. Martellucci, "A new prediction model of rain attenuation that separately accounts for stratiform and convective rain," *IEEE Transactions on Antennas and Propagation*, Vol 57, No. 1, January 2009, Page(s): 196 - 204.

[4] L. Luini, C. Riva, C. Capsoni, A. Martellucci, "Attenuation in non rainy conditions at millimeter wavelengths: assessment of a procedure," *IEEE Trans. Geosci. Remote Sens.*, vol. 45 (7), pp. 2150-2157, July 2007.

[5] E. R. Westwater, F. O. Guiraud, "Ground-based microwave radiometric retrieval of precipitable water vapor in the presence of clouds with high liquid content," *Radio Science*, vol. 15, pp. 947-957, 1980.

[6] http://www.ecmwf.int, Website of the European Centre for Medium-Range Weather Forecasts.

[7] COST Action 255 Final Report, Chapter 3.2, "Precipitation, clouds and other related non-refractive effects," Editor J.P.V. Poiares Baptista, ESA Publication Division, The Netherlands, ISSN: 0379-6566, ISBN: 92-9092-608-2255.

[8] http://www.usgs.gov/, Website of the United States Geological Survey.

[9] International Organization for Standardization, Standard Atmosphere, ISO 2533:1975, 1975.

[10] E. W. Danielson, J. Levin, E. Abrams, "Meteorology," McGraw Hill, 2003.

[11] J. A. Goff, S. Gratch, "Low-pressure properties of water from −160 to 212 °F," *in Transactions of the American Society of Heating and Ventilating Engineers*, pp 95–122, presented at the 52nd annual meeting of the American Society of Heating and Ventilating Engineers, New York, 1946.

[12] E. Salonen, W. Uppala, "New Prediction method of cloud attenuation," *Electr. Lett.*, 27 (12), pp. 1106-1108, 1991.

[13] H. J. Liebe, G. A. Hufford, M. G. Cotton, "Propagation modelling of moist air and suspended water/ice particles at frequencies below 1000 GHz," *AGARD 52nd Specialists' Meeting of The EM Wave Propagation Panel*, Palma De Maiorca, Spain, 1993.

[14] J. Nessel, J. Morse, M. Zemba, C. Riva, L. Luini, "Preliminary results of the NASA beacon receiver for Alphasat Aldo Paraboni TDP5 propagation experiment," *the 20th Ka and BroadBand Communications, Navigation and Earth Observation Conference*, Vietri, Italy, October 1-3, 2014, pp. 357-365.

[15] A. V. Bosisio, C. Capsoni, "Brightness temperature ratios: Analysis of typical behaviour," *in Proc. IGARSS*, 1995, vol. 2, p. 1133.